

Research Article

Cytotoxicity of Silver Nanoparticles in Human Embryonic Stem Cell-Derived Fibroblasts and an L-929 Cell Line

Hui Peng,¹ Xuehui Zhang,¹ Yan Wei,¹ Wentao Liu,¹ Shenglin Li,^{2,3} Guangyan Yu,⁴ Xin Fu,⁵ Tong Cao,⁵ and Xuliang Deng¹

¹Department of Geriatric Dentistry, Peking University School and Hospital of Stomatology, Beijing 100081, China

²Central Laboratory, Peking University School and Hospital of Stomatology, Beijing 100081, China

³Laboratory of Oral and Maxillofacial Surgery, Peking University School and Hospital of Stomatology, Beijing 100081, China

⁴Department of Oral and Maxillofacial Surgery, Peking University School and Hospital of Stomatology, Beijing 100081, China

⁵Faculty of Dentistry Research Laboratories, National University of Singapore, Singapore 119083

Correspondence should be addressed to Xuliang Deng, kqdengxuliang@bjmu.edu.cn

Received 4 April 2012; Accepted 20 May 2012

Academic Editor: Xiaoming Li

Copyright © 2012 Hui Peng et al. This is an open access article distributed under the Creative Commons Attribution License, which permits unrestricted use, distribution, and reproduction in any medium, provided the original work is properly cited.

Consensus about the toxicity of silver nanoparticles (Ag-NPs) has not been reached, even though extensive attention has been paid to this issue. This confusion may be due to physicochemical factors of Ag-NPs and the cell model used for biological safety evaluation. In the present study, human embryonic stem cell-derived fibroblasts (EBFs), which have been considered a closer representative of the *in vivo* response, were used as a novel cell model to assess the cytotoxicity of Ag-NPs (~20 nm and ~100 nm) in comparison with L-929 fibroblast cell line. Cell proliferation, cell cycle, apoptosis, p53 expression, and cellular uptake were examined. Results showed that Ag-NPs presented higher cytotoxicity to EBF than to L-929. EBF demonstrated a stronger capacity to ingest Ag-NPs, a higher G2/M arrest, and more upregulated p53 expression after exposed to Ag-NPs for 48 h when compared with L-929. It could be concluded that EBF exhibited a more sensitive response to Ag-NPs compared with L-929 cells, indicating that EBF may be a valid candidate for cytotoxicity screening assays of nanoparticles.

1. Introduction

The unique physicochemical properties of nanomaterials have allowed their rapid progress and acceptance into nanobiotechnology and life science. There are reports that silver nanoparticles (Ag-NPs) have been widely accepted in catheters [1], wound dressings [2], and the clothing and food industry [3] due to their efficacy as antimicrobial agents. Despite this progress, their potential adverse effects on human health and the environment have not yet been elaborately elucidated, and their biocompatibility remains controversial.

Ag-NPs may translocate to the circulatory system and distribute throughout the main organs of the body, especially the kidney, liver, and brain [4], and they can penetrate the blood-testis and blood-brain barriers [5]. This observation implies that Ag-NPs could become neurotoxic and genotoxic [4]. A Previous study has reported that 15 nm Ag-NPs

could lead to drastically reduced mitochondrial function and cell viability of mouse spermatogonial stem cells at concentration of 5–10 $\mu\text{g}/\text{mL}$ [6]. Hussain et al. [7] reported that 15 nm Ag-NPs exhibited significant cytotoxicity at 10–50 $\mu\text{g}/\text{mL}$ in the BRL 3 A cell line. Other studies have also reported adverse cellular reactions of Ag-NPs to other cell types, such as NIH3T3, vascular smooth muscle cells [8], and mouse embryonic stem cells [9]. But inconsistency, such as different toxic concentration, indeed exists among the results of numerous cytotoxicity studies, which may be ascribed to the varied cell models used in the evaluation of Ag-NPs cytotoxicity to a certain degree.

Recently, embryonic stem cells (ESCs) have gained great attention and showed multiple potential in tissue regeneration, drug screening, and biomaterial cytotoxicity test [10, 11]. With the development of methodologies for obtaining cells derived from human ESCs (hESCs), several advantages of the differentiated progenies from hESCs have been

reported. Unlike immortalized cell lines, which are usually of cancerous origin, containing chromosomal and genetic aberrations that produce immortality, and highly accustomed to *in vitro* culture conditions after countless passages, hESCs have been demonstrated to be genetically and karyotypically normal, which would make them more representative of how a normal cell should behave *in vivo*. Nowadays, several established hESC lines are readily available, from which an almost limitless supply of differentiated somatic progenies can be obtained. Furthermore, differentiated somatic progenies are expected to show little inter-batch variability, provided *in vitro* culture and differentiation protocols are well standardized [12]. Therefore, we proposed the hypothesis that differentiated somatic progenies derived from hESCs may be advantageous in the evaluation of Ag-NPs toxicity and may be used as a novel option in nanocytotoxicity studies.

This study was planned to study the cytotoxicity of Ag-NPs (~ 20 nm and ~ 100 nm) to human embryonic stem cell-derived fibroblasts (EBFs) in comparison with L-929 cell line. Cell proliferation, cell cycle, apoptosis, p53 expression, and cellular uptake were examined. Whether EBF could be a valid candidate as a cell model for cytotoxicity screening of Ag-NPs or not was analyzed.

2. Materials and Methods

2.1. Materials and Chemicals. Ag-NPs with two different sizes, that is, Ag-NPs-1 (~ 20 nm) and Ag-NPs-2 (~ 100 nm), were provided by Hongwu Nanomaterial Co. Ltd. (Xuzhou, China). L-929 cells were obtained from the American Type Cell Culture Collection (ATCC, Rockville, MD, USA). Dulbecco's Modified Eagle's Medium (DMEM), RPMI 1640, fetal bovine serum (FBS), antibiotic agent (penicillin-streptomycin, PS), trypsin-EDTA, DMEM/F-12, knockout serum replacement, nonessential amino acid, and L-glutamine were purchased from Gibco (Grand Island, NY, USA). Basic fibroblast growth factor (bFGF) was obtained from Invitrogen (Carlsbad, CA, USA). β -mercaptoethanol was provided by Sigma-Aldrich (St. Louis, MO, USA). Annexin-V-FLUOS staining kit was purchased from Roche Molecular Biochemicals (Mannheim, Germany). Cell Counting Kit-8 (CCK-8) was purchased from Dojindo Laboratories (Tokyo, Japan). All other chemical solvents were of analytical grade with no further purification.

2.2. Characterization of Ag-NPs. Scanning electron microscopy (SEM), transmission electron microscope (TEM), and energy-dispersive X-ray spectroscopy (EDX) analysis were used to characterize the size, morphology, distribution, and chemical purity of the Ag-NPs.

2.3. Cell Culture. The NIH-registered hESC line, H9, was obtained from the National University of Singapore. H9 cells were cultured on a layer of mitomycin C-inactivated mouse embryonic fibroblasts (MEFs) in ESC medium (Table 1) at 37°C with 5% CO_2 atmosphere and 95% humidity. H9 cells were digested with 1 mg/mL collagenase IV, scraped down from MEF feeder layers, and cultured as embryonic bodies (EBs) in suspension with EB medium (Table 1) for

5 days. Then, the EBs were transferred to a new flask coated with 0.1% gelatin and cultured with differentiation medium (Table 1). EBs differentiated spontaneously to fibroblast-like cells, named EBF cells. EBF and L-929 cells were, respectively, cultured in DMEM and RPMI 1640. Cells were maintained at 37°C in a 5% CO_2 atmosphere and 95% humidity. The cells were subcultivated when they reached 80% confluency.

2.4. In Vitro Assay for Cytotoxic Activity of Ag-NPs

2.4.1. Cell Viability Assay. Cell viability was quantified using a CCK-8 assay as per manufacturer's protocol. In brief, cells were seeded in 96 well plates at a density of 1×10^4 cells ($200 \mu\text{L}/\text{well}$) followed by overnight incubation. The supernatant was then aspirated from the well, and fresh aliquots of growth medium (containing Ag-NPs in concentration of 0.5, 5, 50, and $500 \mu\text{g}/\text{mL}$) after ultrasonic dispersion were added. After 24, 48, and 72 h, the supernatant was again aspirated, and cell monolayers were washed with PBS. Subsequently, water-soluble tetrazolium (WST) reagent ($20 \mu\text{L}$) was added in each well, incubated for 4 h, centrifuged, the supernatant obtained, and absorbance at two wavelengths (415 nm and 630 nm) was recorded using a microplate reader (Bio-Rad 680, Microplate Master, Hercules, CA, USA). The effect of nanoparticles on cells was expressed as the percentage of cell viability compared with the controls or relative proliferation rate (RPR), which is calculated as the following formula: $\text{RPR} (\%) = (A - A_N) / A_N \times 100\%$, where A represents the absorbance of each different concentration group; A_N is the absorbance of negative control group.

2.4.2. Cell Cycle Analysis. Cell cycle analysis was carried out by propidium iodide (PI) staining followed by flow cytometry measurement of the fluorescence. Approximately, 1×10^5 cells were placed in cell culture flask. Following treatment with Ag-NPs ($50 \mu\text{g}/\text{mL}$) for 24, 48, and 72 h, the medium was removed and stored. Cells were washed in PBS, trypsinized, harvested in the stored medium, and centrifuged. The pellet was washed, fixed in ice-cold ethanol (70%), and stored at -20°C . Before flow cytometry analysis, cells were washed in PBS and stained with PI in RNase ($50 \mu\text{g}/\text{mL}$ PI and $0.25 \text{ mg}/\text{mL}$ RNase A) and incubated at 37°C for 1 h, followed by incubation at 4°C until analysis. Flow cytometry analysis was performed using BD FACS Calibur (BD Biosciences) at an excitation wavelength of 488 nm and emission wavelength of 610 nm. Data collected for 1×10^6 cells was analyzed using CellQuest software 6.0 (BD Biosciences).

2.4.3. Annexin-V Staining Apoptosis Analysis. Annexin-V staining was performed to analyze apoptosis induced by Ag-NPs. Cells were treated with $50 \mu\text{g}/\text{mL}$ Ag-NPs for 48 h. Cell preparation and experimental procedures were as for cell cycle analysis. The staining was performed as per manufacturer's instructions. Data analyses were performed using Cell Quest software 6.0.

TABLE 1: The component of cells culture medium.

Cells culture medium	Component
ESC medium	DMEM/F-12 supplemented with 20% knockout serum replacement, 4 ng/mL bFGF, 1 mmol/L L-glutamine, 1% non essential amino acid, and 0.1 mmol/L β -mercaptoethanol
EB medium	DMEM/F-12 supplemented with 20% knockout serum replacement, 1 mmol/L L-glutamine, 1% non essential amino acid, and 0.1 mmol/L β -mercaptoethanol
Differentiation medium	DMEM, 1 mmol/L L-glutamine and 10% FBS
EBF medium	DMEM containing 10 units/mL penicillin, 10 units/mL streptomycin and, 10% FBS
L-929 medium	RPMI 1640 containing 10 units/mL penicillin, 10 units/mL streptomycin, and 10% FBS

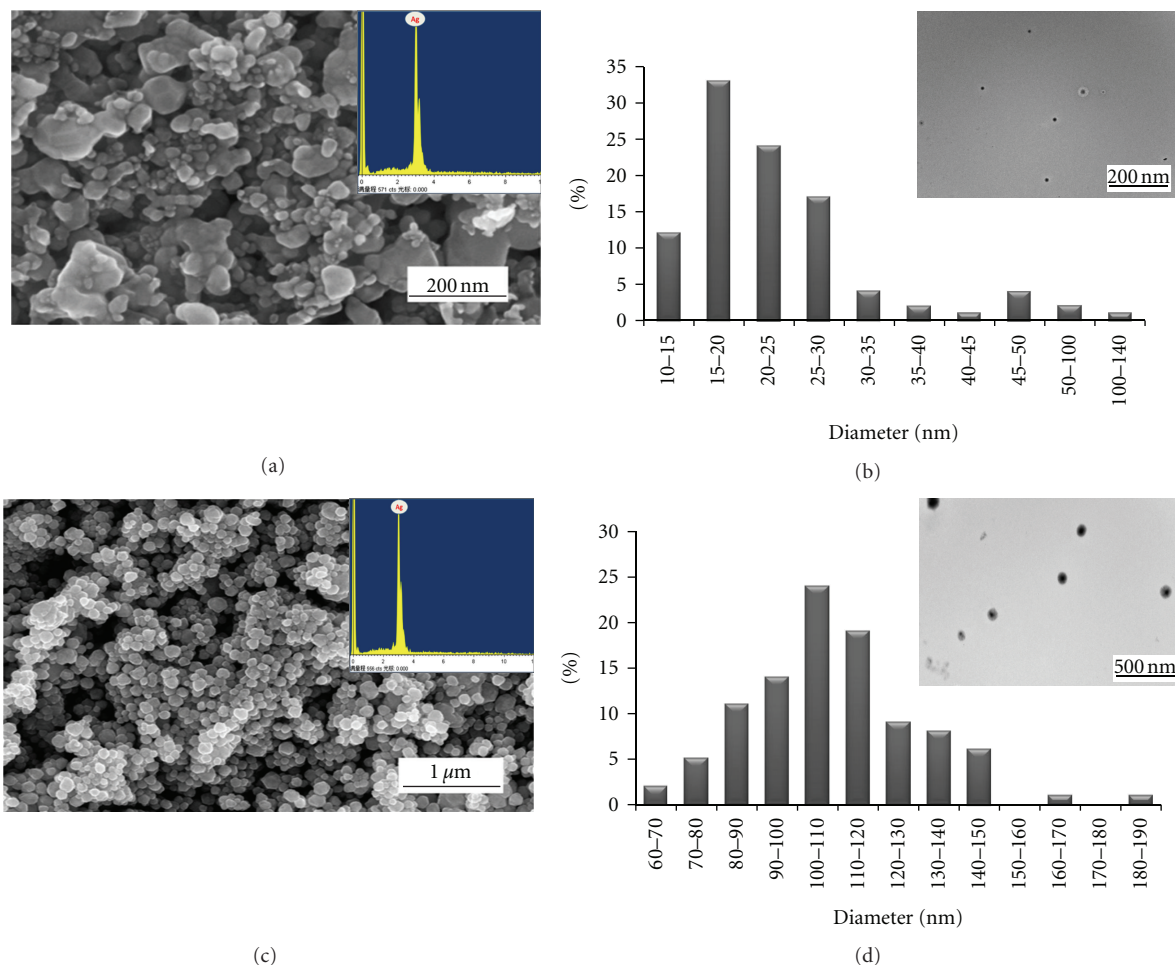


FIGURE 1: Characterization of Ag-NPs by SEM, EDX and TEM: (a) Ag-NPs-1 SEM with DEX image, (b) size distribution histogram and TEM image of Ag-NPs-1, (c) Ag-NPs-2 SEM with DEX images, (d) size distribution histogram and TEM image of Ag-NPs-2.

2.5. Cellular Uptake and Quantitative Determination of the Uptake of Ag-NPs. Ultrathin sections of cells were analyzed using TEM to reveal the uptake and distribution of NPs. Briefly, the cells (1.5×10^6) were treated with Ag-NPs ($50 \mu\text{g/mL}$) for 48 h. At the end of the incubation period, culture flasks were washed many times with PBS to remove excess unbound NPs. Cells were trypsinized and fixed in 2.5% glutaraldehyde for 2 h. Fixed cells were washed with PBS. Postfixation staining was achieved using 1% osmium tetroxide for 1 h at room temperature. Cells were washed well, dehydrated in alcohol, and treated with propylene oxide

for 30 min, followed by treatment with propylene oxide, Spurr's low viscosity resin (1 : 1) for 18 h. Cells were further treated with pure resin for 24 h and embedded in BEEM capsules containing pure resin. Resin blocks were hardened at 70°C for 2 days. Ultrathin sections (70 nm) were cut using an ultramicrotome (Lecia EM UC6). The sections were stained with 1% lead citrate and 0.5% uranyl acetate and analyzed under transmission electron microscope examination (H-7650B, Hitachi, Japan).

Subconfluent cells were incubated at 37°C in the presence or absence of $50 \mu\text{g/mL}$ Ag-NPs for 24 h under cell culture

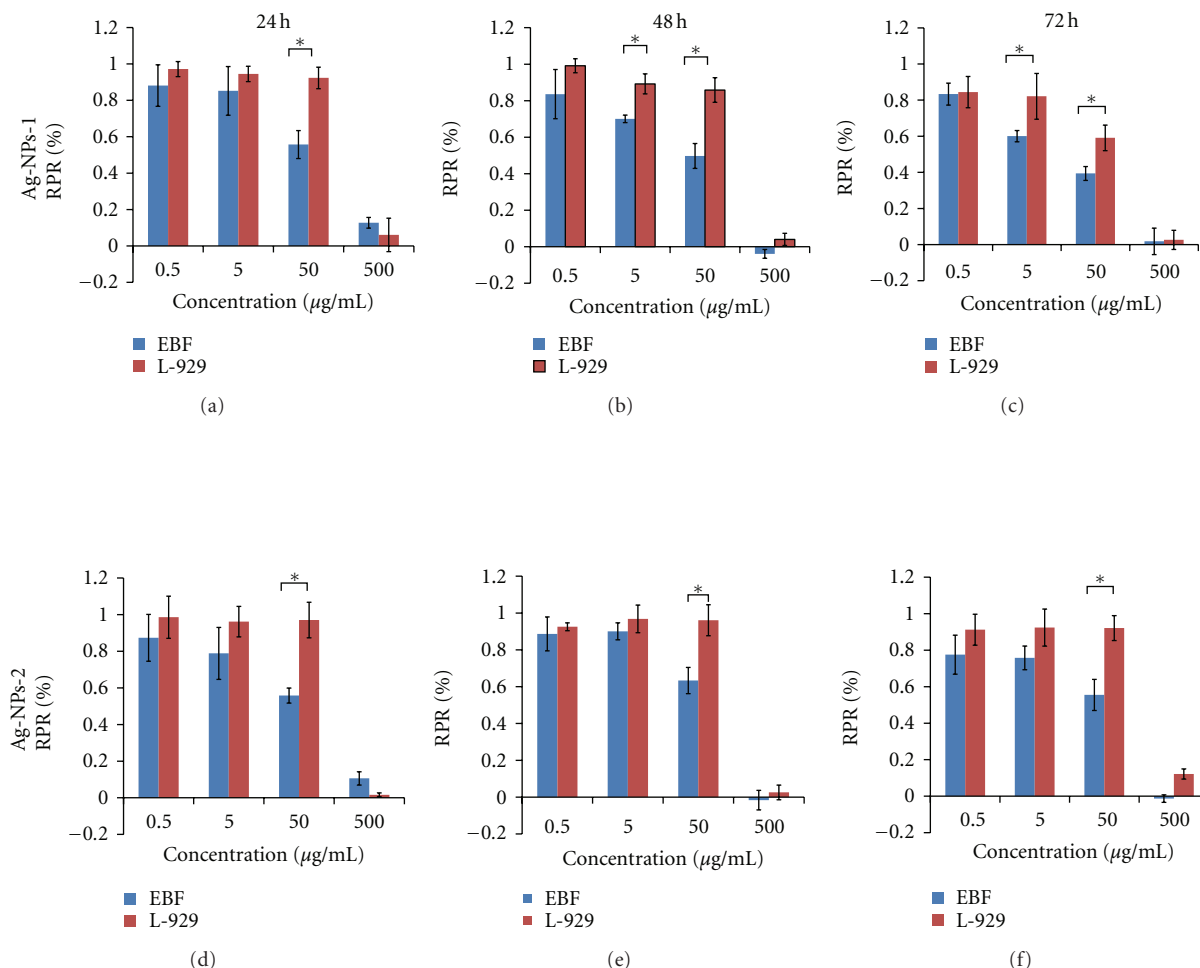


FIGURE 2: Cytotoxicity assay of EBF and L-929 cells after treatment with Ag-NPs (0.5–500 µg/mL) for 24, 48, and 72 h. (a) Ag-NPs-1 24 h, (b) Ag-NPs-1 48 h, (c) Ag-NPs-1 72 h, (d) Ag-NPs-2 24 h, (e) Ag-NPs-2 48 h, (f) Ag-NPs-2 72 h. *Astatistically significant difference between EBF and L-929 cells ($P < 0.05$).

conditions. Subsequently, the cells were washed with PBS, detached with trypsin and suspended in medium. The uptake of particles into cells was analyzed using flow cytometry. The side scatter data were analyzed using CELL Quest 6.0 software. Calibration reagents and solutions for flow cytometry were from Becton Dickinson. Ten thousand cells were acquired for each measurement.

2.6. Real-Time Quantitative-Polymerase Chain Reaction (RTq-PCR). To assess DNA damage associated with the Ag-NPs, the level of p53 expression in cells was detected using RTq-PCR. The cells were seeded with 1×10^5 cells/dish and cultured with the 50 µg/mL Ag-NPs solution for 48 h. Total RNA was isolated with TRIZOL Reagent (Invitrogen) and was reverse transcribed using an iScript cDNA synthesis kit (Bio-Rad Laboratories). RTq-PCR was performed with a two-step RTq-PCR kit (Invitrogen) according to the manufacturer's instructions. The mRNA expression of p53, an important signaling molecule in checkpoint responses to DNA damage [13], was detected after treatment by a 7500 real-time PCR System (Applied Biosystems) with the SYBR

TABLE 2: Primers used for RTq-PCR.

Gene Name	Sequence
p53-human-R	CCGCAGTCAGATCCTAGCG
p53-human-F	AATCATCCATTGCTTGGGACG
p53-mouse-R	GTCACAGCACATGACGGAGG
p53-mouse-F	TCTTCCAGATGCTCGGGATAC
GAPDH-human-R	AGGGGCCATCCACAGTCTTC
GAPDH-human-F	AGAAGGCTGGGGCTCATTG
GAPDH-mouse-R	GCTCCTGGAAGAGGTGAT
GAPDH-mouse-F	TCGTCCCGTAGACAAAATG

Premix Ex Taq Perfect Real Time kit (Takara Mirus Bio, Madison, WI). The sequences of the primer pairs are shown in Table 2.

2.7. Statistical Analysis. All experiments were performed in duplicate and repeated at least three times. The statistical significance of the data was expressed as mean \pm SD. Statistical

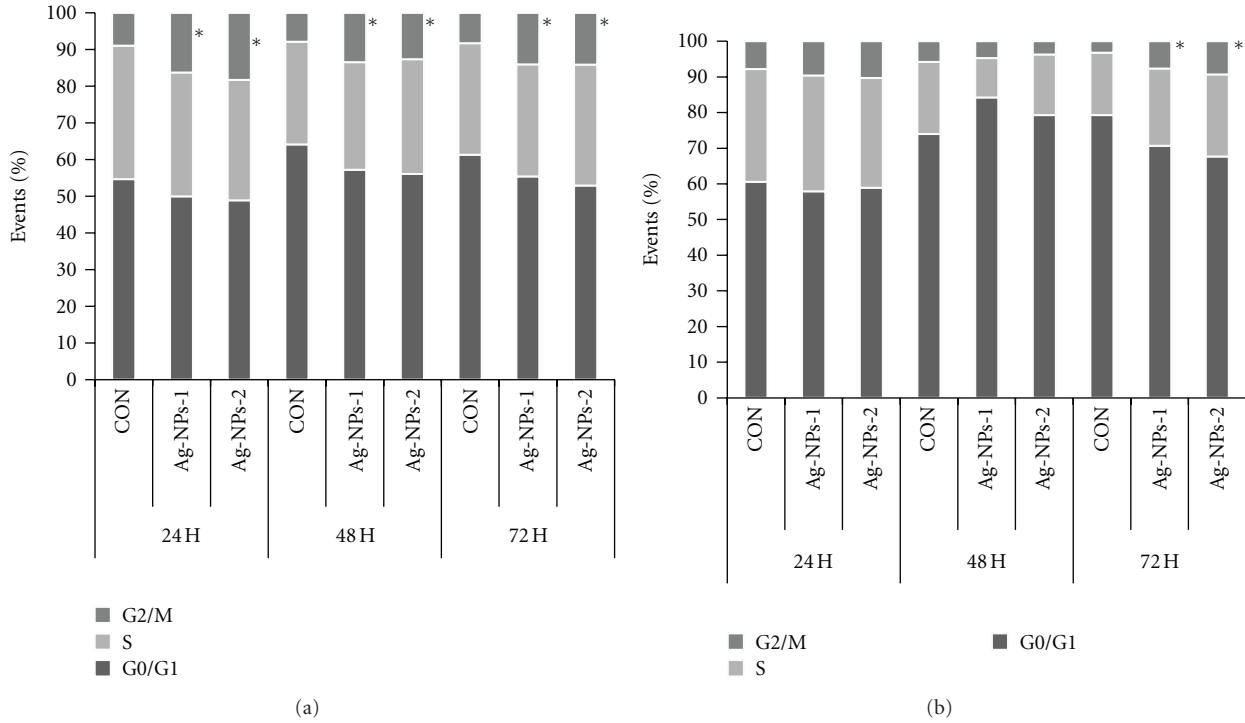


FIGURE 3: Cell cycle population of EBF (a) and L-929 cells (b) after treatment with Ag-NPs-1 and Ag-NPs-2.

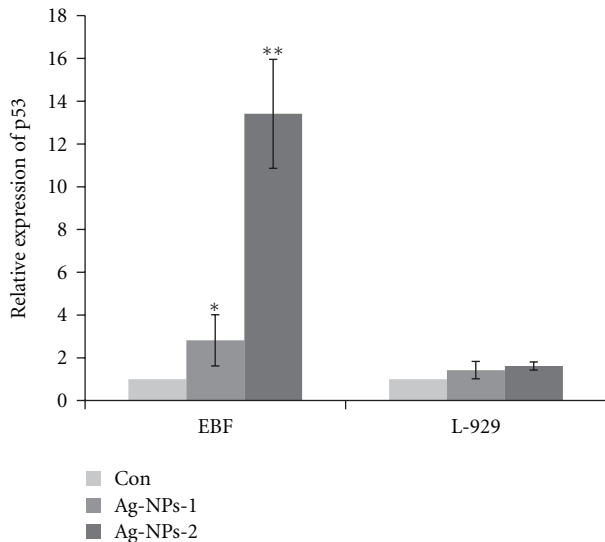


FIGURE 4: Expression of p53 in EBF and L-929 following Ag-NPs exposure for 48 h. *Significant differences in comparison with control group ($P < 0.05$). **Highly significant differences in comparison with control group ($P < 0.01$).

differences between groups were evaluated by Student t -test using the software SPSS 13.0 (SPSS Science). P values of less than 0.05 were considered to be statistically significant.

3. Results and Discussion

3.1. Characterization of Ag-NPs. Both kinds of Ag-NPs were observed to be spherical in shape (Figures 1(a) and 1(c)

under SEM, with average size of $20 \text{ nm} \pm 12.6 \text{ nm}$ (Ag-NPs-1, Figure 1(b)) and $100 \pm 21.3 \text{ nm}$ (Ag-NPs-2, Figure 1(d)), as measured by software Image J (National Institutes of Health, USA). EDX results demonstrated that the nanoparticles were 100% pure silver. TEM image showed the even distribution of Ag-NPs dispersed in water.

3.2. Cytotoxicity of Ag-NPs

3.2.1. Cell Viability of EBF and L-929 Cells. Cell viability was quantified using a CCK-8 assay. Figure 2 displays the RPR of EBF and L-929 cells after 24, 48, and 72 h exposure to Ag-NPs-1 and Ag-NPs-2 at concentration of 0.5–500 $\mu\text{g}/\text{mL}$. The RPR were decreased in a dose-dependent manner and the RPR of EBF treated with Ag-NPs of both size were lower than that of L-929 cells at the same concentration and time point. 50 $\mu\text{g}/\text{mL}$ was shown the threshold concentration that significantly inhibited EBF proliferation, and this concentration was used in all subsequent experiments including cell cycle analysis, apoptosis assay, cellular uptake, and p53 expression. When the NPs concentration reached 500 $\mu\text{g}/\text{mL}$, nearly no viable cells existed. CCK-8 results also showed apparent size-dependent cytotoxic effects on cell proliferation. The RPR of EBF treated with Ag-NPs-1 was lower than that of Ag-NPs-2 at 5–50 $\mu\text{g}/\text{mL}$, both at 48 and 72 h. However, the size-dependent cytotoxic effects on L-929 cells occurred only at 50 $\mu\text{g}/\text{mL}$ after 72 h exposure in this study. These results indicated that EBF may be more vulnerable to Ag-NPs treatment when compared with L-929 cell line.

The dose-dependent toxicity pattern of Ag-NPs was consistent with previous studies on mammalian germline stem cells [6] and may be due to the impact of endocytosis

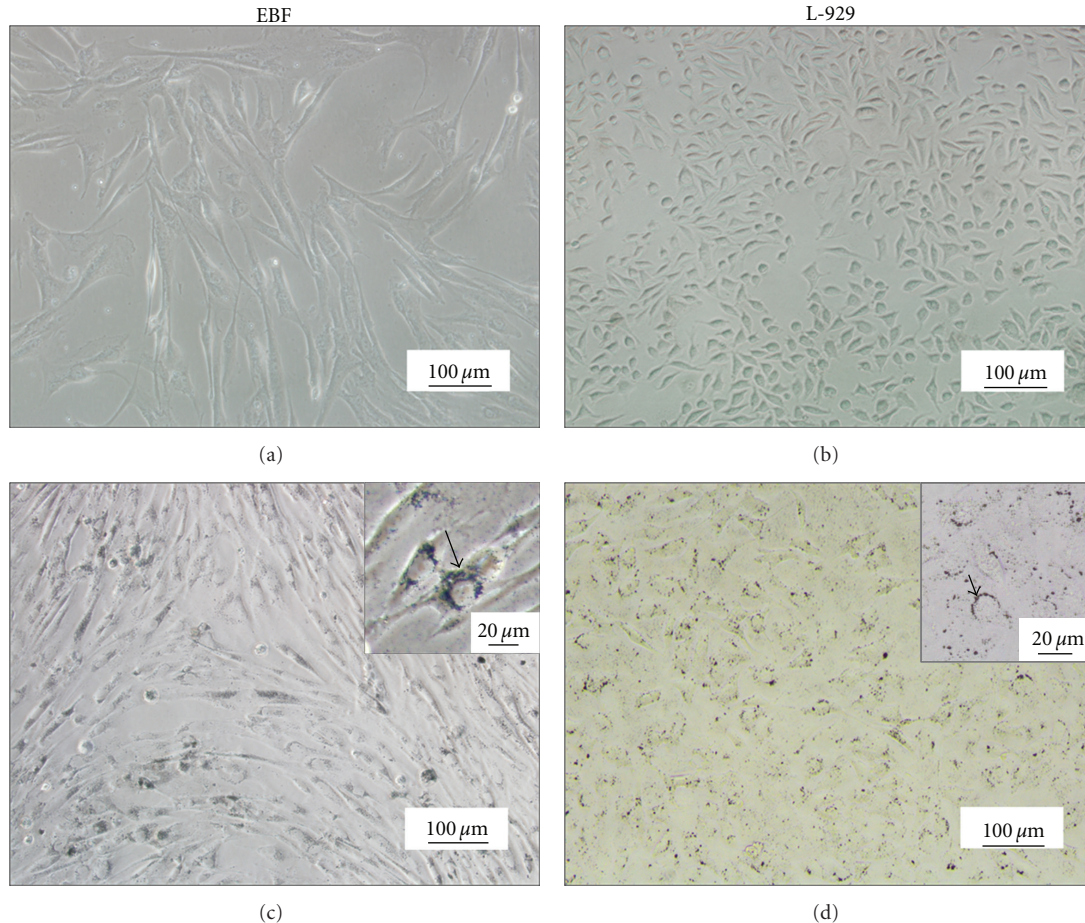


FIGURE 5: Phase-contrast micrographs (magnification 200x) of EBF and L-929 cells before (a) and (b) and after (c) and (d) treatment with Ag-NPs-1 at 50 µg/mL for 48 h. The insets show the high magnification (magnification 400x).

and metabolism inhibiting normal cellular activity at larger concentrations of Ag-NPs. The results in our study that cell proliferation in EBF was more sensitive to Ag-NPs give evidence for a cell-type-dependent response in biomaterials cytotoxicity test. Similarly, Cao et al. [14] reported that mitomycin C decreased EBF viability more obviously than L-929 cells and considered that EBF were more sensitive than L-929 cells in cytotoxicity screening tests. Tedja et al. [15] noticed that the different level of biological response should be primarily attributed to the difference in the amount of cellular particle uptake between different cell types. Hence, the cell-type-specific response of cells to Ag-NPs here could be due to that EBF are genetically and karyotypically normal and exhibited a stronger capacity to ingest NPs (Figure 7). Previous studies have also indicated that Ag-NPs have a size-dependent cytotoxicity, with smaller particles being more toxic [16, 17]. According to Carlson et al. [18], Ag-15 nm and Ag-30 nm NPs showed more cytotoxicity than that of Ag-55 nm. Our study revealed similar findings that the RPR of EBF and L-929 cells treated with Ag-NPs-1 was lower than that with Ag-NPs-2. The reason may be that smaller Ag-NPs have a larger surface area available for interaction and lead to a stronger effect than larger particles [19].

3.2.2. Cell Cycle Analysis. The influence of NPs on the cell cycle was analyzed by subjecting the NP-treated cells to flow cytometry. In control group, major cell populations were observed in the G1 phase, whereas in Ag-NPs treated cells, a decrease in the G1 cell population was accompanied by an increase in the G2/M cell population (Figure 3). The G2/M population of Ag-NPs treated EBF cells were significantly increased to almost twice the control values at 24, 48, and 72 h (Figure 3(a)). G2/M arrest of L-929 cells was observed at 72 h (Figure 3(b)). DNA damage was proposed to be the main cause of cell cycle arrest [20]. AshaRani et al. [21] reported oxidative stress in Ag-NPs treated cells indicating the possibility of DNA damage and chromosomal aberrations which was considered the prime factors resulting in cell cycle arrest. The results in this study indicated that EBF cells may be more vulnerable to Ag-NPs than the L-929 cell line.

3.2.3. Apoptosis and DNA Damage Induced by Ag-NPs. Annexin-V staining indicated that the rate of EBF cells apoptosis was increased from $0.77 \pm 0.08\%$ (control) to $2.88 \pm 0.23\%$ (Ag-NPs-1) and $1.49 \pm 0.33\%$ (Ag-NPs-2) at 50 µg/mL, whereas that of L-929 cells treated with the

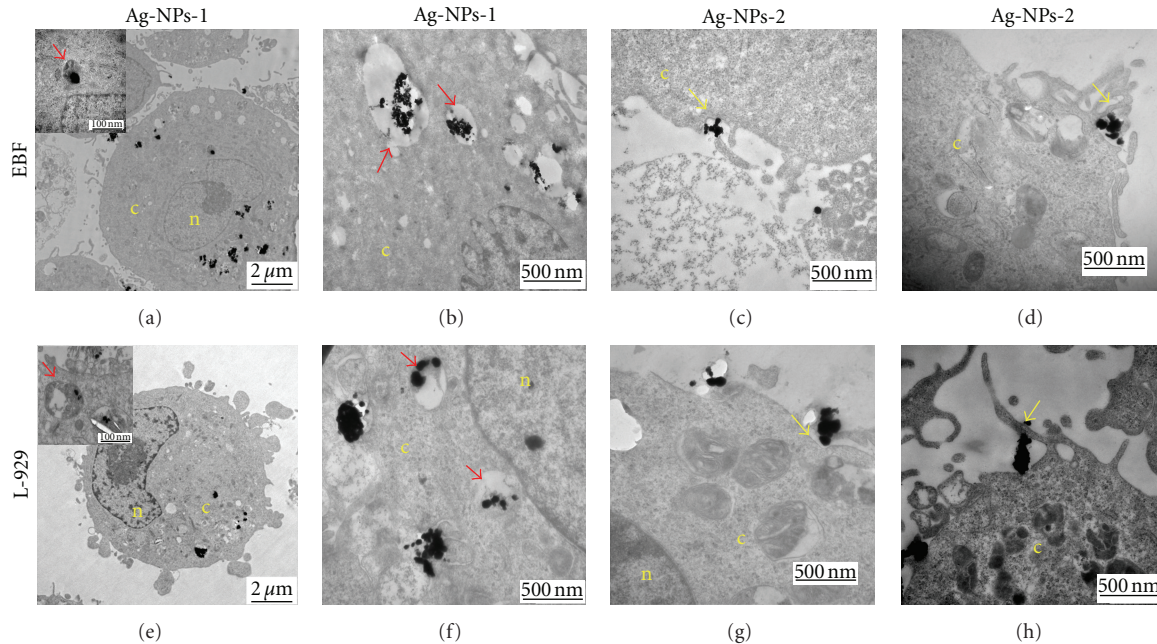


FIGURE 6: TEM images of ultrathin sections of EBF (a)-(d) and L-929 (e)-(h) cells treated with Ag-NPs after 48 h. Nanoparticles were showed inside the cytoplasm (c), but they were not in the nucleus (n) of both cell types. Cells showed large endosomes (a) and (e) and lysosomes (b) and (f) with nanoparticles inside (red arrow). Invagination (c) and (g) and protrusion (d) and (h) of the plasma membrane were observed when Ag-NPs attached the cells (yellow arrow).

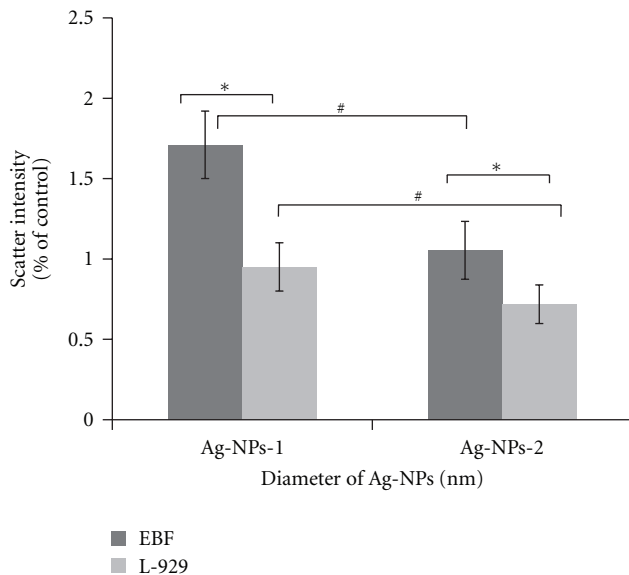


FIGURE 7: Intracellular occurrence of Ag-NPs agglomerates analyzed using flow cytometric light scatter. *Significant differences between EBF and L-929 cells ($P < 0.05$). #Significant differences between Ag-NPs-1 and Ag-NPs-2 groups.

same concentration of Ag-NPs had no significant change compared with the control (Table 3). This result showed that the impact of early apoptosis, at the concentration of Ag-NPs selected in our study, was not apparent, but the value

TABLE 3: The rate of apoptosis treated with Ag-NPs.

	Control	Ag-NPs-1	Ag-NPs-2
EBF	0.77 ± 0.08	$2.88 \pm 0.23^*$	$1.49 \pm 0.33^*$
L-929	0.63 ± 0.13	0.74 ± 0.09	0.67 ± 0.29

* $P < 0.05$ compared with control.

did show that Ag-NPs might cause EBF apoptosis. In the presence of DNA damage, p53 accumulates and triggers cell cycle arrest to provide time for the damage to be repaired [22]. Therefore, p53 expression could be assessed by RTq-PCR to monitor the DNA damage indirectly. Data in Figure 4 showed that expression of p53 in EBF cells treated with both sized Ag-NPs within 48 h increased significantly. Especially in Ag-NPs-2 treated EBF cells, their p53 expression even reached almost 14 times of the control group. While the changes observed in the L-929 cells were not statistically significant (Figure 4). Ahamed et al. [9] have also indicated that Ag-NPs up-regulated p53, Rad51 and phosphorylated-H2AX expression. This observation supported the hypothesis that Ag-NPs can cause DNA damage and resulted in G2/M cell cycle arrest, which may be correlated to long-term effects, such as mutagenesis or carcinogenesis [23].

3.3. Cellular Uptake and Distribution of Ag-NPs. Under phase-contrast microscopy, Ag-NPs were observed in the cytoplasm of both cell types and gathered in the perinucleus.

Single or clustered NPs were attached to the cell membrane and were internalized into cells (Figures 5(c) and 5(d)). TEM images also showed that the NPs were distributed throughout the cytoplasm, but they were not observed in the nucleus of both cell types (Figures 6(a) and 6(e)). According to the TEM images, there were no significant differences in cellular uptake between the two cell types. Large endosomes and lysosomes with Ag-NPs were also observed (Figures 6(a), 6(b), 6(e), and 6(f)). Invagination of plasma membranes (Figures 6(c) and 6(g)) denoted the endocytosis of nanomaterials. The protrusion of the plasma membrane (Figures 6(d) and 6(h)) for uptake of the nanospheres indicated the characteristics of endocytosis and macropinocytosis. These results suggested that Ag-NPs were entering the cells through pinocytosis rather than diffusion. Greulich et al. [24] have reported that the uptake of PVP-coated Ag-NPs was significantly inhibited by chlorpromazine and wortmannin, suggesting endocytosis and macropinocytosis were the primary uptake mechanisms.

The uptake of nanomaterials depended not only on the particle size and charge, but also on the cell type [25]. The quantitative uptake of Ag-NPs was determined by analysis of the intracellular side scatter signal using flow cytometry. As Figure 7 demonstrated, EBF had the stronger uptake capacity of Ag-NPs compared with L-929 cells. The results also showed that both cell types took up more Ag-NPs-1 particles than Ag-NPs-2, which might be due to the smaller diameter and resulted in size-dependent nanotoxicity. The differences in uptake capacity between cell lines can be explained by the differentiation state of the cells. There was report that endocytosis was normally downregulated after treatment of dendritic cells with maturation stimuli [26]. As differentiated progenies from hESCs, EBFs were less mature than L-929 immortalized cells. Hence, it could be reasonable to speculate that the difference between uptake capacity of EBFs and L-929 might be owing to the differing differentiation state. The cellular uptake mechanisms, depending on cell type and particle size, may also be contributed to, or triggered by, the ability of NPs to penetrate the plasma membrane [27]. The uptake of the NPs appears to be quite complicated, therefore, further work is required to elucidate the underlying cellular uptake mechanism elaborately.

4. Conclusion

In this study, the results showed that cytotoxicity of Ag-NPs was dependent on dose, cell type, and particle size. Ag-NPs presented higher cytotoxicity to EBF than to L-929. EBF exhibited an higher G2/M arrest and more upgraded p53 expression after exposed to Ag-NPs for 48 h when compared with L-929. According to the cellular uptake analysis, the NPs were found in the cytoplasm and lysosomes, but they were not observed in the nucleus. EBF demonstrated a stronger capacity to ingest Ag-NPs. According to the results of this study, it could be postulated that EBF was more sensitive to Ag-NPs than L-929. Taking into account of its more representative of how a normal cell should behave *in vivo*, EBF could be considered a promising candidate for cell model of nanomaterials cytotoxicity screening.

Acknowledgments

The authors would like to thank the National University of Singapore for the stem cell resources and Center of Biomedical Analysis at Tsinghua University for the electron microscopy resources. This work was supported by the National Basic Research Program of China (2012CB933904), the National Natural Science Foundation of China (no. 81171000) and International S&T Cooperation Program of China (ISTCP, 2011DFA32190).

References

- [1] U. Samuel and J. P. Guggenbichler, "Prevention of catheter-related infections: the potential of a new nano-silver impregnated catheter," *International Journal of Antimicrobial Agents*, vol. 23, no. 1, supplement 1, pp. S75–S78, 2004.
- [2] J. Chen, C. M. Han, X. W. Lin, Z. J. Tang, and S. J. Su, "Effect of silver nanoparticle dressing on second degree burn wound," *Zhonghua Wai Ke Za Zhi*, vol. 44, no. 1, pp. 50–52, 2006.
- [3] N. Vigneshwaran, A. A. Kathe, P. V. Varadarajan, R. P. Nachane, and R. H. Balasubramanya, "Functional finishing of cotton fabrics using silver nanoparticles," *Journal of Nanoscience and Nanotechnology*, vol. 7, no. 6, pp. 1893–1897, 2007.
- [4] J. Tang, L. Xiong, S. Wang et al., "Distribution, translocation and accumulation of silver nanoparticles in rats," *Journal of Nanoscience and Nanotechnology*, vol. 9, no. 8, pp. 4924–4932, 2009.
- [5] H. S. Sharma, S. Hussain, J. Schlager, S. F. Ali, and A. Sharma, "Influence of nanoparticles on blood-brain barrier permeability and brain edema formation in rats," *Acta Neurochirurgica Supplement*, vol. 106, pp. 359–364, 2010.
- [6] L. Braydich-Stolle, S. Hussain, J. J. Schlager, and M. C. Hofmann, "In vitro cytotoxicity of nanoparticles in mammalian germline stem cells," *Toxicological Sciences*, vol. 88, no. 2, pp. 412–419, 2005.
- [7] S. M. Hussain, K. L. Hess, J. M. Gearhart, K. T. Geiss, and J. J. Schlager, "In vitro toxicity of nanoparticles in BRL 3A rat liver cells," *Toxicology in Vitro*, vol. 19, no. 7, pp. 975–983, 2005.
- [8] Y.-H. Hsin, C.-F. Chen, S. Huang, T.-S. Shih, P.-S. Lai, and P. J. Chueh, "The apoptotic effect of nanosilver is mediated by a ROS- and JNK-dependent mechanism involving the mitochondrial pathway in NIH3T3 cells," *Toxicology Letters*, vol. 179, no. 3, pp. 130–139, 2008.
- [9] M. Ahamed, M. Karns, M. Goodson et al., "DNA damage response to different surface chemistry of silver nanoparticles in mammalian cells," *Toxicology and Applied Pharmacology*, vol. 233, no. 3, pp. 404–410, 2008.
- [10] J. Rohwedel, K. Guan, C. Hegert, and A. M. Wobus, "Embryonic stem cells as an in vitro model for mutagenicity, cytotoxicity and embryotoxicity studies: present state and future prospects," *Toxicology in Vitro*, vol. 15, no. 6, pp. 741–753, 2001.
- [11] H. Spielmann, E. Genschow, G. Scholz et al., "Preliminary results of the ECVAM validation study on three in vitro embryotoxicity tests," *ATLA Alternatives to Laboratory Animals*, vol. 29, no. 3, pp. 301–303, 2001.
- [12] G. Sinha, "Cell biology. Human embryonic stem cells may be toxicology's new best friends," *Science*, vol. 308, no. 5728, p. 1538, 2005.
- [13] A. Sancar, L. A. Lindsey-Boltz, K. Ünsal-Kaçmaz, and S. Linn, "Molecular mechanisms of mammalian DNA repair and the

- DNA damage checkpoints,” *Annual Review of Biochemistry*, vol. 73, pp. 39–85, 2004.
- [14] T. Cao, K. Lu, X. Fu, and B. C. Heng, “Differentiated fibroblastic progenies of human embryonic stem cells for toxicology screening,” *Cloning and Stem Cells*, vol. 10, no. 1, pp. 1–10, 2008.
- [15] R. Tedja, C. Marquis, M. Lim, and R. Amal, “Biological impacts of TiO₂ on human lung cell lines A549 and H1299: particle size distribution effects,” *Journal of Nanoparticle Research*, vol. 13, no. 9, 2011.
- [16] B. Carlson, K. Leschkies, E. S. Aydil, and X. Y. Zhu, “Valence band alignment at cadmium selenide quantum dot and zinc oxide (10 $\bar{1}$) interfaces,” *Journal of Physical Chemistry C*, vol. 112, no. 22, pp. 8419–8423, 2008.
- [17] M. V. Park, A. M. Neigh, J. P. Vermeulen, L. J. de la Fonteyne, H. W. Verharen, J. J. Briede et al., “The effect of particle size on the cytotoxicity, inflammation, developmental toxicity and genotoxicity of silver nanoparticles,” *Biomaterials*, vol. 32, no. 36, pp. 9810–9817, 2011.
- [18] C. Carlson, S. M. Hussein, A. M. Schrand et al., “Unique cellular interaction of silver nanoparticles: size-dependent generation of reactive oxygen species,” *Journal of Physical Chemistry B*, vol. 112, no. 43, pp. 13608–13619, 2008.
- [19] R. C. Doty, T. R. Tshikhudo, M. Brust, and D. G. Fernig, “Extremely stable water-soluble Ag nanoparticles,” *Chemistry of Materials*, vol. 17, no. 18, pp. 4630–4635, 2005.
- [20] M. C. Stensberg, Q. Wei, E. S. McLamore, D. M. Porterfield, A. Wei, and M. S. Sepúlveda, “Toxicological studies on silver nanoparticles: challenges and opportunities in assessment, monitoring and imaging,” *Nanomedicine*, vol. 6, no. 5, pp. 879–898, 2011.
- [21] P. V. AshaRani, G. L. K. Mun, M. P. Hande, and S. Valiyaveetil, “Cytotoxicity and genotoxicity of silver nanoparticles in human cells,” *ACS Nano*, vol. 3, no. 2, pp. 279–290, 2009.
- [22] C. J. Sherr, “Principles of Tumor Suppression,” *Cell*, vol. 116, no. 2, pp. 235–246, 2004.
- [23] R. Paillot, F. Laval, J. C. Audonnet, C. Andreoni, and V. Juillard, “Functional and phenotypic characterization of distinct porcine dendritic cells derived from peripheral blood monocytes,” *Immunology*, vol. 102, no. 4, pp. 396–404, 2001.
- [24] C. Greulich, J. Diendorf, T. Simon, G. Eggeler, M. Epple, and M. Köller, “Uptake and intracellular distribution of silver nanoparticles in human mesenchymal stem cells,” *Acta Biomaterialia*, vol. 7, no. 1, pp. 347–354, 2011.
- [25] L. W. Zhang and N. A. Monteiro-Riviere, “Mechanisms of quantum dot nanoparticle cellular uptake,” *Toxicological Sciences*, vol. 110, no. 1, pp. 138–155, 2009.
- [26] F. Sallusto and A. Lanzavecchia, “Efficient presentation of soluble antigen by cultured human dendritic cells is maintained by granulocyte/macrophage colony-stimulating factor plus interleukin 4 and downregulated by tumor necrosis factor α ,” *Journal of Experimental Medicine*, vol. 179, no. 4, pp. 1109–1118, 1994.
- [27] K. Kostarelos, L. Lacerda, G. Pastorin et al., “Cellular uptake of functionalized carbon nanotubes is independent of functional group and cell type,” *Nature Nanotechnology*, vol. 2, no. 2, pp. 108–113, 2007.